Heliyon 6 (2020) e04111

Contents lists available at ScienceDirect

Heliyon

journal homepage: www.cell.com/heliyon

Research article

Enhancement of antioxidant activity of levan through the formation of nanoparticle systems with metal ions

Rukman Hertadi *, Muzayana Mahbuba Saleha Amari, Enny Ratnaningsih

Biochemistry Research Division, Faculty of Mathematics and Natural Sciences, Institut Teknologi Bandung, Indonesia

ARTICLE INFO

Keywords:
Nanotechnology
Pharmaceutical chemistry
Levan
Metal ion-levan nanoparticle
Antioxidant

ABSTRACT

Levan, a natural polymer, is widely used in biomedical applications, such as antioxidants, anti-inflammatory, and anti-tumor. The present study aimed to enhance the antioxidant activity of levan by combining it with various metal ions in the nanoparticle (NP) system. Levansucrase encoding gene from *Bacillus licheniformis* BK1 has been inserted into an expression vector and the obtained recombinant was labeled as Lsbl-bk1 (accession number MF774877.1). That enzyme was used for *in vitro* levan synthesis in 12% (w/v) sucrose as a substrate and about 4.28 mg/mL of levan was obtained. Levan-based metal ion NPs were synthesized using the coprecipitation method. In the production of NPs, levan acts as a reducing and stabilizing agent. Four types of levan-based metal ion NPs were synthesized, namely, levan–Fe^{2+} NPs, levan–Cu^{+} NPs, levan–Co^{2+} NPs, and levan–Zn^{2+} NPs. The transmission electron microscopy (TEM) technique was applied to visualize the size and shape of the synthesized levan–metal NPs. All levan-based metal ion NPs have a particle size of less than 100 nm, and even levan–Cu^{+} and levan–Zn^{2+} have particle sizes less than 50 nm. Levan–Fe^{2+} NPs and levan–Cu^{+} NPs exhibited prominent antioxidant activity with an inhibition level of up to 88% and 95%, respectively. And the inhibition level of two metal ion NPs had about 33%–40% higher antioxidant activity compared with the inhibition level of levan only. The two levan–metal ion NPs, therefore, have future prospects to be developed as the new formulation for the antioxidant drugs.

1. Introduction

Free radicals, which are unstable compounds that have unpaired electrons, are very reactive because they always try to form electron pair by reacting with other substances (proteins, fats, and DNA) in the body. In certain amounts, free radicals are needed for health to fight inflammation, kill bacteria, and regulate smooth muscle tone in organs and blood vessels. Phagocytes, such as neutrophils, macrophages, and monocytes, release free radicals to destroy invading pathogenic microbes as part of the body's defense mechanism against diseases (Pham-Huy et al., 2008). However, the amount of excessive free radicals can be damaging and very dangerous. Free radicals are formed through normal cell metabolism, inflammation, lack of nutrients, gamma radiation, ultraviolet (UV), environmental pollution, and cigarette smoke. Naturally, the body's antioxidant system as a mechanism of protection against free radical attacks is already present in the body. There are two kinds of antioxidants: internal and external antioxidants. Internal antioxidants are those produced by the body itself. Naturally, the body is able to produce its own antioxidants, but this ability has some limitations. The body's ability to produce natural antioxidants will decrease because of age (Buehler, 2012). Oxidative damage from free radicals in the body can basically be overcome by endogenous antioxidants, such as enzyme catalase, glutathione peroxidase, superoxide dismutase, and glutathione S-transferase (Peng et al., 2014). But if there are excess free radical compounds in the body or if they exceed the limits of cellular antioxidant protection capabilities, additional antioxidants from the outside or exogenous antioxidants are needed to neutralize the formed radicals. The ideal exogenous antioxidant should be easily absorbed and sent to the intracellular location needed to reduce pathological oxidative damage. To develop effective antioxidants, the best strategy is to create a new nanoscale drug delivery system because of its size. The nanosized particles which is in the range of 10–100 nm can facilitate the penetration to the tissue system thereby improving the uptake of the drug by the targeted cells (Mirza and Siddiqui, 2014).

Exopolysaccharide is a polysaccharide produced and secreted by microbial cells into the medium (extracellular) (Rehm, 2009). Several types of bacteria, fungi, yeast, and microalgae have been investigated to have the ability to produce exopolysaccharides. The presence of

* Corresponding author.
E-mail address: rukman@chem.itb.ac.id (R. Hertadi).

https://doi.org/10.1016/j.heliyon.2020.e04111
Received 3 April 2020; Received in revised form 16 May 2020; Accepted 28 May 2020

exopolysaccharides is characterized by the growth of mucus in the growth medium of microorganisms (Nwodo and Okoh, 2012). In general, exopolysaccharides produced by these microorganisms have significant biological functions which are as cell protector and preventing cell aggregation (Nicolaus et al., 2010). Levan is a branched exopolysaccharide composed of fructose units with β-(2,6)-glycosidic bonds in the main chain and β-(2,1)-glycosidic bonds in its branching (Liu et al., 2012). Levan has been widely applied in the food industry as a low-calorie prebiotic and sweetener, as well as in the health sector as antidiabetic, antiviral, anti-inflammatory, antitumor, and antioxidant (Kang et al., 2009). Currently levan is also used as material for the manufacture of nanoparticles to encapsulate drugs, catalysts and metal ions (Carlos et al., 2018).

Levan synthesis requires the help of levansucrase biocatalyst (E.C 2.4.1.10), with sucrose as its substrate (Freitas et al., 2011). This enzyme synthesizes levan in three reaction stages, including hydrolysis of sucrose to glucose and fructose, then transfer fructose to sucrose (trans-fructosylation), and the fructose chain extension stage (polymerization) (Badel et al., 2011). Levans can be obtained by direct production of original bacteria or by recombinant techniques (Jathore et al., 2012). However, problems exist in the use of bacteria originating from levan production, such as the level of acquisition of levan which is on a low scale. Isolation and characterization of levansucrase-encoding genes from *Bacillus licheniformis* BK1 were performed and named as Lsbl-bk1 (accession number MF774877.1). The gene was successfully cloned into the pGEM-T Easy Vector in the host *E. coli* TOP10 cell and was also subcloned to the pET-30A expression vector in the *E. coli* BL21 (DE3) plysS host cell. Therefore, the production of recombinant levansucrase from host cell *E. coli* BL21 (DE3) plysS-Lsbl-bk1 was the first step in obtaining biocatalysts to synthesize levan *in vitro*. It is hoped that the production of recombinant levansucrase in optimum conditions can produce a greater amount of levan.

Many researchers have conducted studies of the potential of levan as an antioxidant (Srikanth et al., 2015; Zhao et al., 2018). Further studies on increasing antioxidant activity have been conducted by modifying antioxidant material in terms of particle size. Nano-sized particles have more reactive properties, large surface area, small diffusion distances, and greater adhesion styles (Sarilmiser and Oner, 2014). In addition, levan nanoparticle has been also well-studied by González-Garcinuño et al. (2020) which performed a comprehensive study about levan nanoparticle formation by developing a kinetic model for a self-assembly. The model predicted well the required critical aggregation concentration (CAC) to form nanoparticles. González-Garcinuño et al. (2019) also have studied silver-coated nanoparticles with bactericidal effect and found that levan nanoparticle did not interfere the killing effect of the silver to kill the bacterial targets.

This present study presents that nanotechnology provides new information on the use of levan as an encapsulation material for metal ions which has antioxidant activity to measure NPs to increase those activities. It also demonstrates that the antioxidant activity of metal ion-coated nanoparticles did not interfere by the levan nanoparticle system instead, it was enhanced significantly.

2. Materials and methods

2.1. Materials

Iron(III) chloride ($FeCl_3$), copper(II) nitrate [$Cu(NO_3)_2$], cobalt(III) nitrate [$Co(NO_3)_3$], zinc acetate [$Zn(CH_3COO)_2$], ethanol (C_2H_5OH), 2,2-diphenyl-1-picrylhydrazyl hydrate (DPPH), and 3,5-dinitrosalicyclic acid (DNS) were purchased from Sigma-Aldrich (Singapore), sodium hydroxide (NaOH) from Merck, kanamycin from Bio Basic, and isopropyl-β-D-thiogalactopyranoside from Thermo Fisher Scientific. The growth medium used is Luria-Bertani (LB) medium containing 1% (w/v) tryptone, and 0.5% (w/v) yeast extract was obtained from Liofilchem, 1% (w/v) NaCl from Merck. The composition of the phosphate buffer solution used was Na_2HPO_4 1 M and $NaH_2PO_4.H_2O$ 1 M, phenol, and H_2SO_4 97% were from Merck. All the chemicals used for the experiments were of analytical grade. All the solutions were prepared by using deionized water, and the glassware was properly washed and autoclaved before conducting the experiments.

2.2. Bacterial strains

The bacterial strains *Escherichia coli* BL21(DE3)plysS carrying pET-*Lsbl*-bk1 used was from the stock culture maintained in our laboratory on LB medium which already contains 50 μg/mL kanamycin antibiotics (selective medium). This recombinant clone contains the levansucrase gene from *Bacillus licheniformis* BK1 (deposited at GenBank NCBI with the accession number of MF774877.1).

2.3. Production and characterization of levan in vitro

Production of levan *in vitro* was following the procedure by Srikanth et al. (2015) with modification. The transformant *E. coli* BL21(DE3), carrying pET-*lsbl-bk1*, was inoculated into 100 mL LB medium containing 50 μg kanamycin and incubated at 37 °C. Enzyme expression was induced by adding 1 mM IPTG when the optical cell density (OD_{600}) of the culture reached 0.6–1.0. The expressed enzyme excreted extracellularly and separated from the cell by centrifugation at 8000 rpm for 15 min. Levan production *in vitro* was performed by mixing 50 mL of the crude recombinant levansucrase Lsbl-bk1 30 μg/mL with 50 mL sucrose solutions 12% (w/v) dissolved in 50 mM phosphate buffer pH 7 and incubated at 37 °C for 18 h. That reaction was stopped by heating at 100 °C for 5 min and then cooled down to room temperature. The precipitated impurities were discarded by centrifugation at 8,000 rpm for 15 min. Levan was obtained by precipitating the supernatant with 95% cold ethanol in a ratio of 1:3. Then, the pellet was freeze-dried for 4 h to obtain dry levan. The concentration of levan was determined by the phenol-sulfuric method at 490 nm using fructose as the standard. Levan was characterized using FTIR. And then the FTIR spectra of levan were compared with the FTIR spectra of pure levan from *Erwinia herbicola*.

2.4. Synthesis of levan-based metal ion nanoparticles

Levan-based metal ion nanoparticles (levan–metal NPs) were synthesized using coprecipitation methods, following the procedure by Pudovkin et al. (2018). In the production of nanoparticles, levan acts as a reducing and stabilizing agent. The metal ions which were used to be coated with levan in this study were Fe^{2+}, Cu^{+}, Co^{2+}, and Zn^{+}. Therefore, to obtain these metal ions, the metal solutions with a higher oxidation number were chosen, such as $FeCl_3$, $Cu(NO_3)_2$, $Co(NO_3)_3$, and $Zn(CH_3COO)_2$, respectively. These metal ions were chosen because they are easily oxidized and has been applied as an antibacterial in the form of nanoparticles (Valgimigli et al., 2018). For each metal, 25 mg levan was dissolved in 25 mL NaOH 0.2% (w/v) in a nutshell. Then, levan solutions were mixed with 25 mL metal solutions of 100 mM, at room temperature, 500 rpm, for 10 min. The mixture then slowly heated at 100 °C for 4 h or until a color change occurs. The color product obtained was centrifuged at 8000 rpm for 15 min and washed three times with distilled water. The precipitate was collected and freeze-dried for 4 h for further analysis.

2.5. Characterization of levan-based metal ion nanoparticles

All of the levan-based metal NPs was characterized using UV–Vis spectroscopy to observe the maximum wavelength from metal NP solution colors and FTIR (*Fourier transform* infrared) to observe the changes in levan wavelength before and after binding metal ions. The morphology and individual size of levan-metal NPs were analyzed using TEM (*transition electron microscopy*). The composition of metal ions from levan-based metal NPs was analyzed using EDS (*energy-dispersive spectroscopy*).

Table 1. Comparison of wavenumber for levan produced with standard levan from *Erwinia herbicola*.

Wavenumber (cm^{-1})		Functional groups
Levan produced in vitro	Levan standard from *E. herbicola*	
3,340.38	3,346.63	–OH
2,941.02	2,944.06	–C-H
1,671.15	1,659.33	H–O–H
1,460.25	1,472.34	–C–H
1,269.55	1,228.15	–C–OH
1,031.73	1,041.16	Phyranose from sugar
939.74–1,269.55	964.17–1,228.15	Fingerprint of polysaccharide

2.6. UV-Vis spectrophotometric analysis

UV-Vis spectra of the levan-based metal NPs were analyzed by PerkinElmer UV-Vis double beam spectrophotometer. Deionized water was used as blank. The scanning range for each samples was 250–600 nm, operated at a resolution of 1 nm.

2.7. Fourier transform infrared (FTIR) spectroscopy

FTIR spectrum of levan, levan–Fe^{2+} NPs, levan–Zn^{2+} NPs, levan–Cu^{+} NPs, and levan–Co^{2+} NPs was recorded using PerkinElmer Spectrum BX, FT-IR (PerkinElmer, Akron, OH, USA) at room temperature through potassium bromide pellet method. A total of 10 mg of NPs, metal salt, and levan were mixed with 10 mg of solid KBr, then it mixed well and pelletized using a vacuum pump. The pellet was kept in IR path and spectrum was measured in the 400–4,000 cm-1 range. FTIR spectroscopy measurements were carried out to recognize the biogroups that are attached on the surface of each samples.

2.8. Transmission electron microscopy (TEM) analysis

The morphology and particle size of levan-based metal ion nanoparticles were analyzed using TEM (Hitachi Model H-7500, Ltd., Tokyo, Japan) with an acceleration voltage of 100 kV. Firstly, the sample solution was sonicated for 10 min. Then, drop on a small of the sample solution was insulated in plate. The morphology of the particles was observed at 100,000x magnification.

2.9. Energy-dispersive spectroscopy (EDS) analysis

The composition of metal ions from levan-based metal NPs was analyzed using EDS (Hitachi Model SU3500, format EDS, manufactured by EDAX from AMETEK, Inc). Analysis using EDS was carried out to see the composition of metal elements contained in levan-based metal ion nanoparticles. A little solid of levan-based metal ion nanoparticles is taken and placed on a carbon adhesive. Then the sample was coated in gold (Au) with a power of 10 mA for 20 min. The composition of metal elements were analysed with an acceleration voltage of 10 kV at 500 magnification.

2.10. Analysis of levan-based metal ion nanoparticle stability

Stability analysis on these NPs was determined using the AAS method. The stability analysis of levan-based metal ion NPs was determined by calculating the levels of metal ions that were successfully encapsulated in the levan-based metal ion NP system and then calculating the levels of loose metal ions in levan-based metal ion NP solutions. Solids NPs were dissolved in demineralized water and stirred then left for a few minutes. Then, the solution of the NPs measured the concentration of metal ions by observing the standard curves of each metal ion.

2.11. Antioxidant activity

The antioxidant activity was measured using the 2,2-diphenyl-1-picrylhydrazyl hydrate (DPPH) assay. The main standard compound used was ascorbic acid, which has high antioxidant activity. Briefly, 750 µL ascorbic acid, levan, all of the levan-based metal NPs, and all of the metal ions at different concentrations were added into 250 µL of the DPPH solution (0.4 mM, dissolved in 95% ethanol, v/v) in microtubes 1.5 mL. The mixture was stirred for 10 s to dissolve all of the components. The solution was incubated at room temperature for 30 min in a dark room. The changes in color from purple to yellow were measured at 518 nm using spectrophotometer UV–Vis. The antioxidant activity was measured based on inhibition percentage as follows:

$$\%\text{Inhibition} = \frac{A_{control} - A_{sample}}{A_{control}} \times 100\% \quad (1)$$

where $A_{control}$ is the absorbance in the absence of the DPPH solution, and A_{sample} is the absorbance in the presence of the sample. Then, a curve was made based on percent inhibition with variations in concentration and the IC_{50} value was calculated. The IC_{50} is defined as the concentration of antioxidants needed to reduce radical DPPH by 50%.

2.12. Statistical analysis

All data were expressed as mean ± standard error of mean (n = 5) and analyzed using one-way analysis of variance (ANOVA), followed by Dunnett's test.

3. Results and discussion

3.1. Production and characterization of levan

The levan mass obtained from a production medium of 100 mL using 12% (w/v) sucrose substrate with 30 µg/mL crude recombinant levansucrase Lsbl-bk1 was 4.28 mg/mL. In the same condition, the levan mass obtained *in vitro* using recombinant Lsbl-bk1 levansucrase was still smaller compared to the levan obtained using recombinant levansucrase L8-37-0-1, which was 6.5 mg/mL. It may be caused by Lsbl-bk1 used in synthesizing levan *in vitro* has not been purified. The FTIR analysis could prove and confirm that the product obtained was levan, as can be seen from the possible functional groups responsible. The levan structure has several distinctive bonds that appeared on the IR spectrum. A significant peak typical for levan is the OH vibration peak at wavenumber

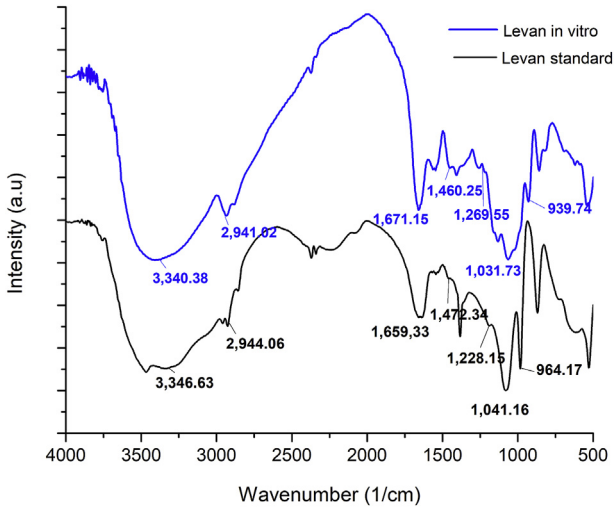

Figure 1. Comparison of the FTIR spectra for levan *in vitro* (——) and standard levan from *Erwinia herbicola* (——).

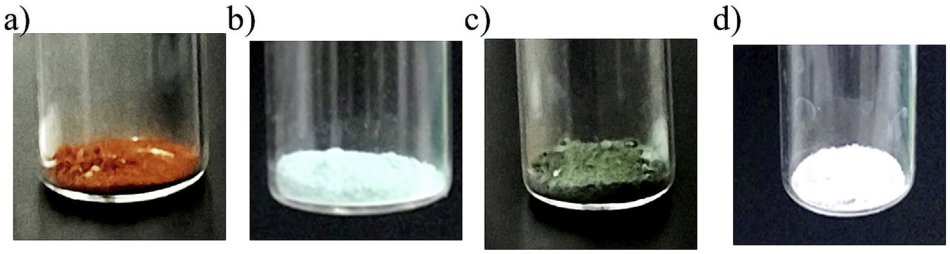

Figure 2. The solids colors of levan–metal NPs. a) Levan–Zn^{2+}, b) levan–Fe^{2+}, c) levan–Co^{2+}, d) levan–Cu^{+}, and e) levan produced.

3600–3200 cm^{-1}, –C–H vibration peak at wavenumber 3000–2800 cm^{-1}, vibration peak C = O at wavenumber 1641–1600 cm^{-1}, and absorption peak for glycosidic bonds at wavenumber 2900 cm^{-1}. Comparing the IR spectrum of levan production results with the standard levan, it can be seen that there are similarities in the spectrum at significant peaks (see Table 1). The levan structure has several distinctive bonds that can appear on the IR spectrum so that it becomes a qualitative analysis to show the real levan product obtained. The FTIR spectra (Figure 1) of levan was referenced according to levan from *Erwinia herbicola* showed: characteristic broad stretching peak of O–H stretching around 3,340.38/cm, weak C–H vibration were observed at around 2,941.02/cm, H–O–H scissors at 1,671.15/cm are of residual water, C–H bending was observed at 1,460.25/cm, and C–OH stretch was observed at 1,269.55/cm. The absorptions at 1,031.73/cm indicated a pyranose form of sugars (Zhao et al., 2005). The wavelength region 939.74–1, 031.73/cm is reported to be fingerprint of molecule because it allows the identification of major chemical groups in polysaccharide (Fellah et al., 2009). The phenolic sulfuric method for determining the total fructant in the levan obtained.

3.2. Synthesis and characterization of levan-based metal ion nanoparticles

Levan-based metal ion NPs have been successfully synthesized, namely, levan–Fe^{2+} NPs, levan–Zn^{2+} NPs, levan–Cu^{+} NPs, and levan–Co^{2+} NPs. All of levan-based metal ion NPs have been confirmed qualitatively from the appearance of color precipitate at the end of the reaction. The colors of levan-Fe^{2+}, levan-Zn^{2+}, levan-Cu^{+}, and levan-Co^{2+} NPs were brownish red, white, light blue, and green, respectively. Solids of levan–metal NPs can be seen from Figure 2. Then, colloidal solutions were characterized by UV–Vis spectroscopic analysis. Levan–Fe^{2+} NPs had a brownish red color and had an absorption peak at 301 nm, levan–Zn^{2+} NPs had a white color (288 nm), levan–Cu^{+} NPs had a light blue color (298 nm), and levan–Co^{2+} NPs had a green color (303 nm). Sundaram et al. (2012) has reported that exopolysaccharide-based Fe_3O_4 NPs had a maximum wavelength in the range of 250–350 nm. Murali et al. (2017) also conducted research on ZnO NPs, which had a maximum wavelength of 320 nm. Dobrucka (2018) has also reported that biosynthesized CuO NPs using the extract of *Galeopsidis herba* had a maximum wavelength of 296 nm.

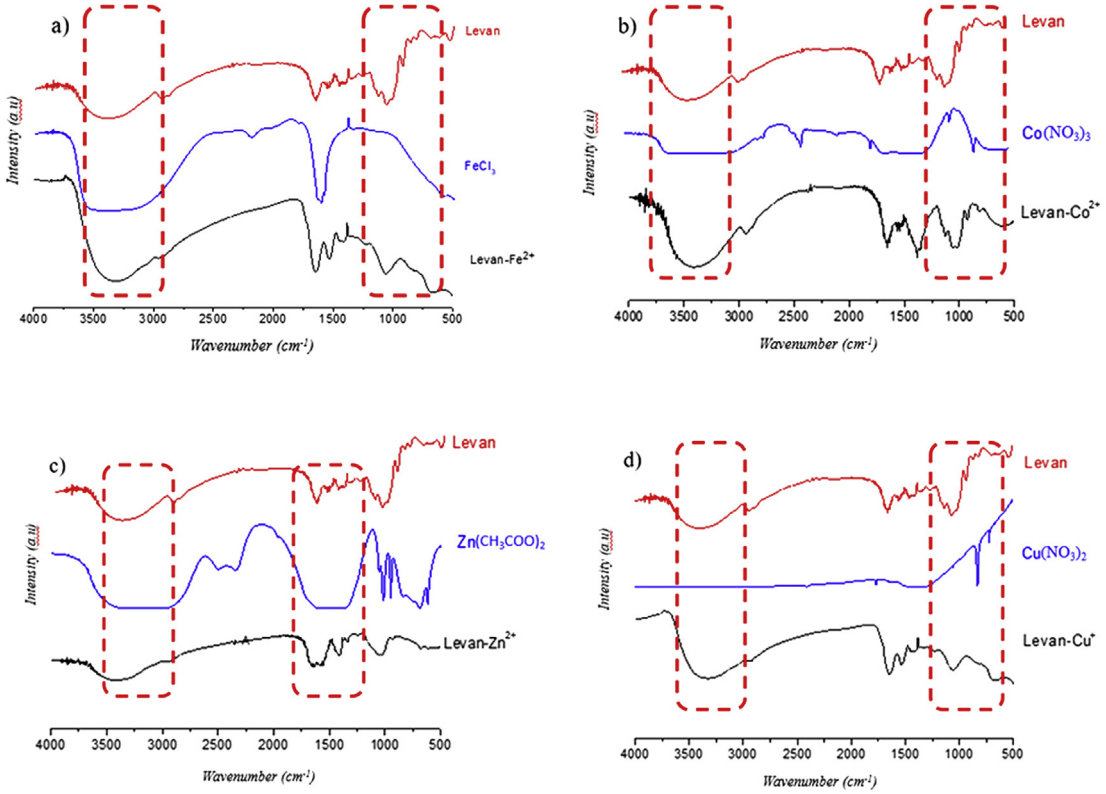

Figure 3. Comparison of the FTIR spectrum for levans, metals, and metal-leached nanoparticles. a) Levan–Fe^{2+}, b) levan–Co^{2+}, c) levan–Zn^{2+}, and d) levan–Cu^{+}.

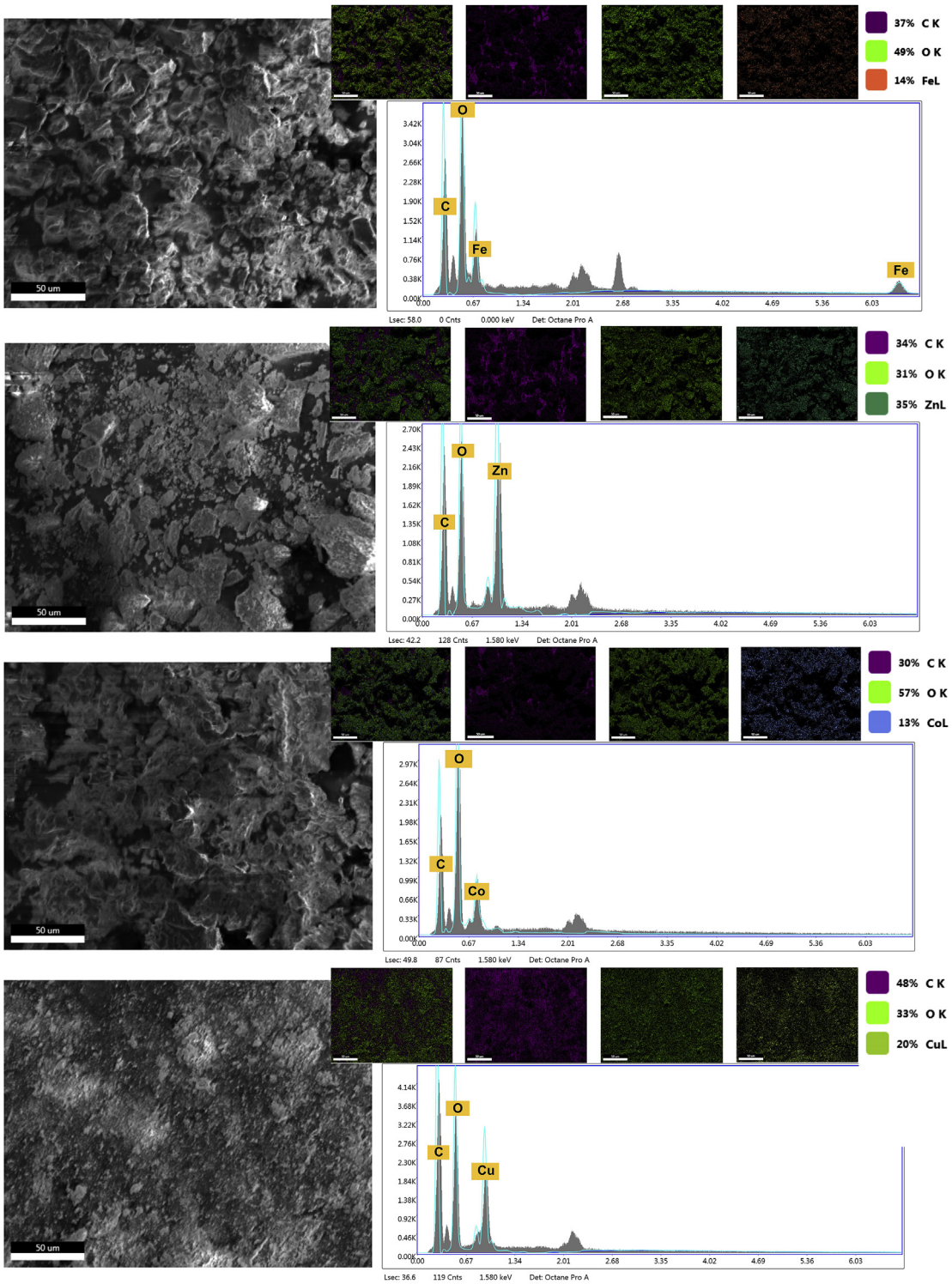

Figure 4. Image and spectrum of EDS mapping results on levan-based metal ion nanoparticles, a) levan produced in vitro, b) levan–Fe^{2+}, c) levan–Cu^{+}, d) levan–Zn^{2+}, and e) levan–Co^{2+}.

The levan modification of metal ions was confirmed using FTIR. The IR spectrum profile in Figure 3 presents the difference in absorption at wavenumbers that are typical for each metal. The FTIR of levan–Fe^{2+} observed in wavenumbers around 3300 cm^{-1}, there is still an O–H vibration from levan, as well as after the formation of elevating NPs with metal. However, at a wavenumber of below 700 cm^{-1}, there is a vibration of Fe metal in the levan–Fe^{2+} spectrum, and the fingerprint of the wavenumber refers to the furanose ring in levan. It can be stated that in the formation of levan-based Fe^{2+} NPs, there is an interaction between the part of the furanose ring and the Fe^{2+} metal ion, which is a similar explanation to that for levan–Co^{2+} and levan–Cu^{+}.

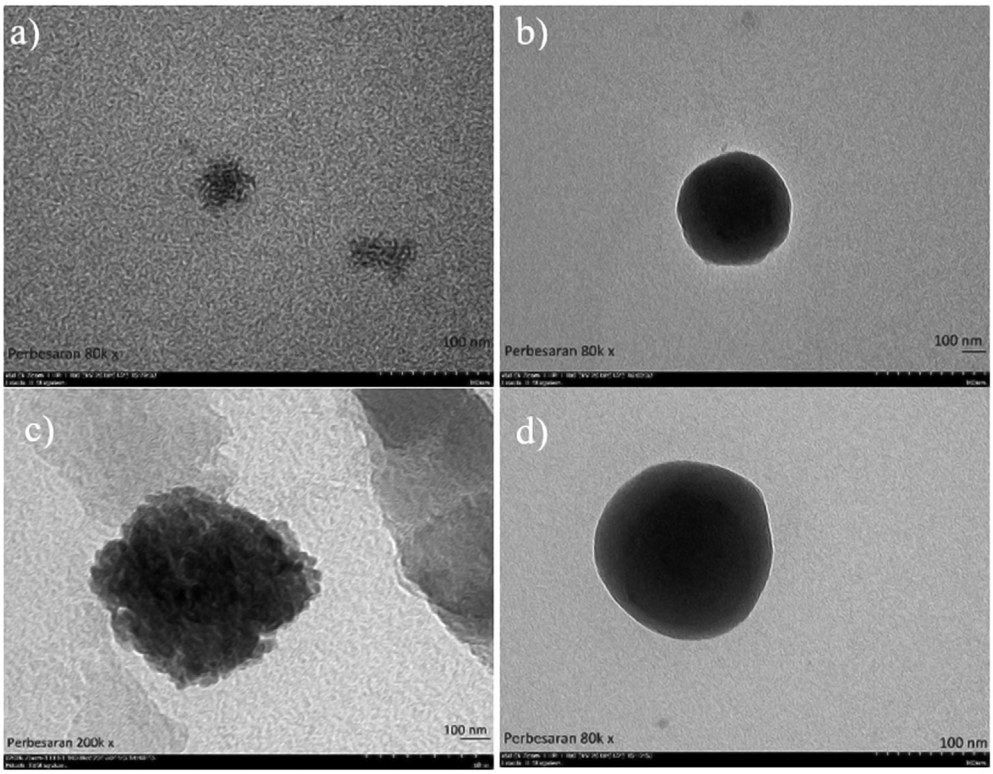

Figure 5. TEM image of levan-based metal ion nanoparticles, a) levan–Cu^{+} NPs, b) levan–Zn^{2+} NPs, c) levan–Co^{2+} NPs, and d) levan–Fe^{2+} NPs.

However, in levan–Zn^{2+}, there are visible spectrum IR differences in the wavenumbers around 1700–1600 cm^{-1}, which show the vibrations of carbonyl or C–O–C in levan. So, it can be said that for levan–Zn^{2+} NPs, levan interacts with metal ions in the glycosidic bond section. The number of metal ion components bound to levan-based metal ion NPs can be analyzed using EDS.

The EDS results from levan-based metal ion NPs can be seen from Figure 4. Based on the analysis of the EDS results, the readable elements on the sample surface for all levan-based metal ion NPs are carbon (C), oxygen (O), and the metal itself. This shows that the levan system has been formed (the element of carbon and oxygen), as well as the metal ions. In addition, in Figure 3, there is also a difference in the color of each readable element, and it can be observed that in levan–Fe^{2+}, the metal content of Fe was only 14%, whereas the oxygen content was 49%. From the image of the elemental position in the EDS levan–Fe^{2+} NPs result, it can also be seen that Fe was in the inside of the sample, which is marked with orange (showing the Fe element) covered by green (oxygen component) and purple (carbon component). The explanation for levan–Zn^{2+} NPs, levan–Cu^{+} NPs, and levan–Co^{2+} NPs resembles the analysis of levan–Fe^{2+} NPs.

The morphology and size of levan-based metal ion NPs were analyzed using TEM (see Figure 5). Before the analysis, the sample was first modified to ensure that the particles were properly separated. So, the results obtained can determine the morphology and particle size of the sample. Levan–Fe^{2+} NPs, levan–Zn^{2+} NPs, and levan–Cu^{+} NPs have a spherical morphology compared with irregular levan–Co^{2+} NPs. This indicates that there are different molecular geometries between levan-based metal ion NPs. Thus, the ability of levan to encapsulate different types of metal ions affects the geometry of the NPs system formed. Based on the results of this TEM, levan is sufficient to encapsulate Zn^{2+} and Fe^{2+} ions, as evidenced by the neatly rounded surface of the NPs. However, all levan-based metal ion NPs have a particle size of less than 100 nm, and even levan–Cu^{+} and levan–Zn^{2+} have particle sizes of less than 50 nm. Thus, levan is quite promising to be used as a material for creating NP systems.

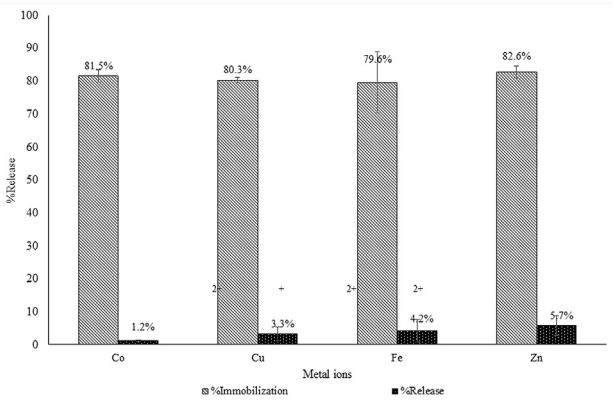

Figure 6. The percent curve of the metal ions in levan-based metal ion nanoparticles (indicated by the stripe motif box) and the stability of levan-based metal ion nanoparticles (indicated by black spots on white spots).

3.3. Stability of levan-based metal ion nanoparticles

The results of metal ion levels and the stability of levan-based metal ion NPs can be seen from Figure 6. Based on these data, it can be seen that all metal ions have about 80% bound to levans. The stability of levan-

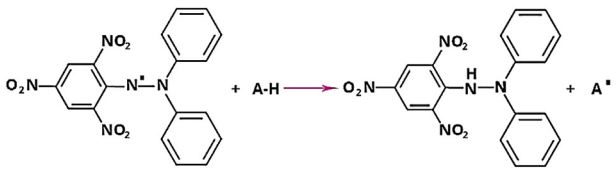

Figure 7. Reaction of DPPH with ascorbic acid.

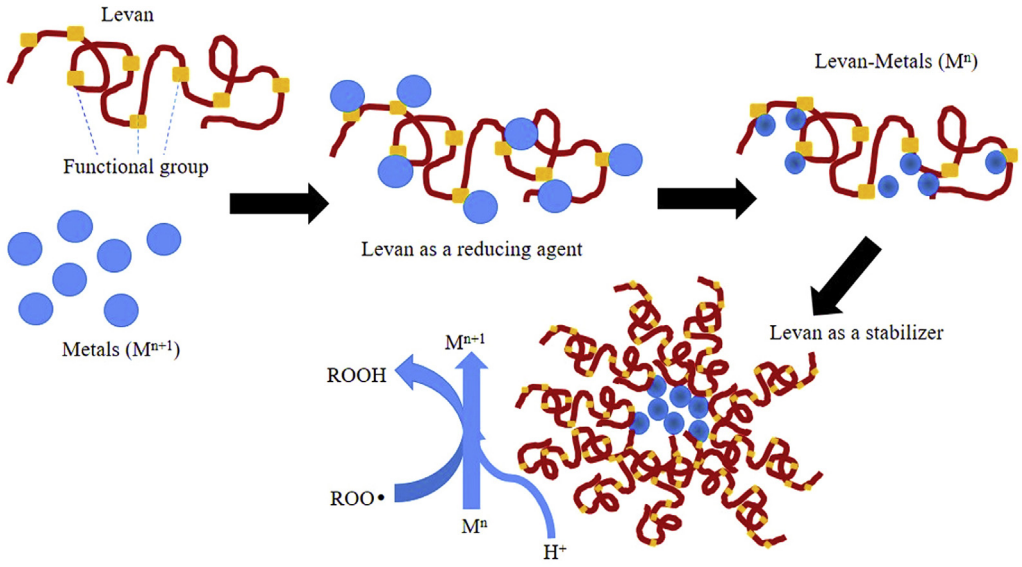

Figure 8. Mechanism of levan-based metal ion nanoparticle production and their role as an antioxidant.

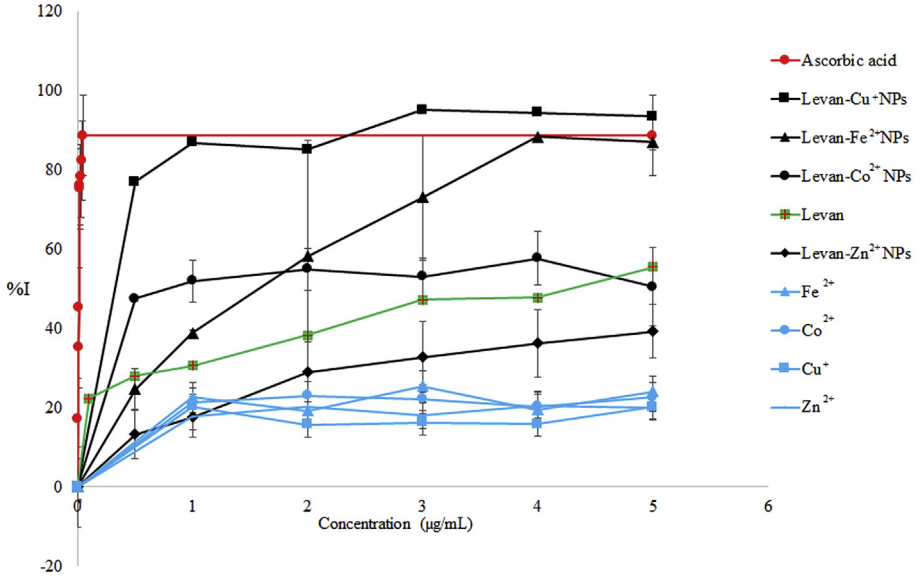

Figure 9. Percent inhibition of free radical compounds for the determination of antioxidant activity in levan-based metal ion nanoparticles (black line), levan only (green line), and ascorbic acid standard (red line).

based metal ion NPs is seen from the percentage of release measured from the concentration of metal ions after dissolving in aqua and a few minutes. According to the results, all levan-based metal ion NPs are quite stable with a percentage of metal ion release of less than 5%.

3.4. Antioxidant activity

The antioxidant activity of levan-based metal ion NPs was determined using DPPH compounds. Basically, the general reaction that occurs in the determination of antioxidant activity using DPPH, reaction with ascorbic acid, for example, can be seen from Figure 7. DPPH radical compounds that are purple when oxidized will experience a change in color to yellow. Then, it is used to determine the antioxidant activity of each sample. In the formation of levan-based metal ion NPs, levan acts as a reducing and stabilizing agent. An illustration of the formation of levan-based metal ion NPs can be seen from Figure 8. Levan has a –OH functional group that can interact with metal ions. In this context, functional groups in their structure that can serve as reductive and stabilizing agents in the synthesis of metal nanoparticles by a chelating and capping process (Escarcega-Gonzales et al., 2018). This interaction results in a reduction in metal ions. The metal ions used in this study were Fe^{3+}, Cu^{2+}, Co^{3+}, and Zn^{2+}. Based on the reduction potential;

$$Co^{3+} + e^- \rightarrow Co^{2+} \quad E^o = +1.80 \text{ V}$$

$$Fe^{3+} + e^- \rightarrow Fe^{2+} \quad E^o = +0.77 \text{ V}$$

$$Cu^{2+} + e^- \rightarrow Cu^{+} \quad E^o = +0.153 \text{ V}$$

$$Zn^{2+} + 2e^- \rightarrow Zn \quad E^o = -0.762 \text{ V}$$

The reduced from of each metal ion encapsulated with levan has the potential to increase antioxidant activity. This phenomenon is explained by the value of the potential reduction energy of each metal ion. Co^{2+}, Fe^{2+}, and Cu^{+} have negative potential energy values, so that they are spontaneous enough to experience oxidation to Co^{3+}, Fe^{3+}, and Cu^{2+}, respectively. It is observed that levan acts as a reducing agent in the manufacture of levan-based metal ion NPs. Based on the data analysis of

one-way ANOVA for the antioxidant activity of only levan, metal ions only, and levan–metal NPs exhibited a significant difference in each of the metal ions, except for Zn^{2+} metal ions which were not significantly different.

The results of the testing of the antioxidant activity between standard compounds, only levan, only metals, and levan-based metal ion NPs, can be seen from Figure 9. Without levan, the antioxidant activity of metal ions were lower. So, the interaction with levan could increase the antioxidant activity of those metal ions. Red curves with round symbols show the antioxidant results of ascorbic acid. It can be seen that at small concentrations (<0.1 mg/mL), ascorbic acid has been able to act as an antioxidant until, finally, it reaches an inhibition of 85% of free radical compounds. In addition, other new samples provide antioxidant properties at a concentration of 0.5 mg/mL. Levan itself has antioxidant properties that can inhibit radical compounds up to 58%. Kim and Chung (2016) hypothesized that levan has antioxidant activity because it contains many hydroxyl groups. The hydroxyl functional groups, which can react with free radicals and terminate radical chain reactions, are highly related to the antioxidant activity. Moreover, several previous studies reported that levan and its derivatives have antioxidant activity (Liu et al., 2012). Metal ions (Fe^{2+}, Cu^{+}, Co^{2+}, and Zn^{2+}) also provide antioxidant properties that can inhibit radical compounds up to 22%. So, a combination of levan and some metal ions which have antioxidant activity is used. The combination of levans with these metal ions that form levan-based metal ion NPs can increase antioxidant activity by up to 95% in levan-based Cu^{+} NPs (especially for Cu^{+} NPs after 5h), followed by levan-based Fe^{2+} NPs which have a percent inhibition of radical compounds by 85%. So, combining levans with metal ions can increase antioxidant activity by 33%–40%. However, negative results are given on the incorporation of levan with Zn^{2+} ions. A decrease in antioxidant activity due to Zn^{2+} has stabilized, so that oxidation does not easily occur, which results in decreased antioxidant activity after being combined with levan. Efrekhari et al. (2018) mentioned that the reduction of Cu(II) to Cu(I) occurs in the presence of GSH and ascorbic acid, which induces the decomposition of H_2O_2 through Fenton reaction and OH^{-}* generation, leading ultimately to membrane lipid peroxidation.

4. Conclusions

This study focuses on the synthesis of levan using levansucrase resulting from heterologous expression. The synthesis of levan-based metal ion nanoparticles (NPs) aimed to obtain the possibility of increasing the antioxidant activity of the levan itself. Levan has been successfully produced *in vitro* using the Lsbl-bk1 recombinant levansucrase biocatalyst. Characterization of functional groups constitute the levan structure has also been performed through FTIR analysis. Based on the IR levan spectrum profile, the production results obtained a significant IR spectrum profile with a standard pure levan from *Erwinia herbicola*. The use of levan in various fields has been widely reported, but this study focuses on the use of levan as a reducing agent and stabilizer in the manufacture of metal ion NPs for antioxidant activity. Four types of levan-based metal ion NPs have been synthesized, namely, levan–Fe^{2+} NPs, levan–Cu^{+} NPs, levan–Co^{2+} NPs, and levan–Zn^{2+} NPs based on analysis *via* UV–Vis, FTIR, EDS, and TEM. Levan-based metal ion NPs also have high stability and can be measured using the AAS method. Four levan-based metal ion NPs have been synthesized, which have the potential to be used as antioxidants, namely, levan–Fe^{2+} NPs and levan–Cu^{+} NPs, with a percentage of inhibition of radical compounds in the amount of 85% and 95%, respectively. Consequently, the two NPs have the potential to be used as new formulation in antioxidant drugs. In addition, levan–Cu^{+} NPs after 5 h were quite stable and gave a percentage of inhibition of radical compounds greater than that of ascorbic acid, although it takes longer time than ascorbic acid.

4.1. Suggestions

Research related to the kinetic and thermodynamic characteristics of levan-based metal ion nanoparticles which have the potential as antioxidant.

Declarations

Author contribution statement

Rukman Hertadi: Conceived and designed the experiments; Performed the experiments; Contributed reagents, materials, analysis tools or data.

Muzayana Mahbuba Saleha Amari: Performed the experiments; Analyzed and interpreted the data; Wrote the paper.

Enny Ratnaningsih: Conceived and designed the experiments; Contributed reagents, materials, analysis tools or data; Wrote the paper.

Funding Statement

This work is funded by the grant from master thesis reseach funding from the Minister of Research and Technology with the contract number #1172w/I1.C01/PL/2019

Competing interest statement

The authors declare no conflict of interest.

Additional information

No additional information is available for this paper.

Acknowledgements

This work was supported by the Bandung Institute of Technology fast-track program through voucher scholarships given to the author. Also, the author thanked Ms. Nur Umriani Permatasari for collaborating in fulfilling this research data.

References

Badel, S., Bernardi, T., Michaud, P., 2011. New perspectives for *Lactobacilli* exopolysaccharides. Biotechnol. Adv. 29, 54–66.

Buehler, B.A., 2012. The free radical theory of aging and antioxidant supplements: a systematic. Evid. Based Compl. Alternative Med. 17 (3), 218–220.

Carlos, E.E.G., Javier, A.G.C., Augusto, V.R., Ruben, M.R., 2018. Bacterial exopolysaccharides as reducing and/or stabilizing agents during synthesis of metal nanoparticles with biomedical applications. Int. J. Polym. Sci. 7045852.

Dobrucka, R., 2018. Antioxidant and catalytic activity of biosynthesized CuO nanoparticles using extract of *Galeopsidis herba*. J. Inorg. Organomet. Polym. 28, 812–819.

Efrekhari, A., Dizaj, S.M., Chodari, L., Sunar, S., Hasanzadeh, A., Ahmadian, E., Hasanzadeh, M., 2018. The promising future of nano-antioxidant therapy against environmental pollutants induced-toxicities. Biomed. Pharmacother. 103, 1018–1027.

Escarcega-Gonzales, C.E., Garza-Cervantes, J.A., Vazquez-Rodriguez, A., Morones-Ramirez, R.M., 2018. Bacterial exopolysaccharides as reducing and/or stabilizing agents during synthesis of metal nanoparticles with biomedical applications. Int. J. Polym. Sci. 15.

Fellah, A., Anjukandi, P., Waterland, M.R., Williams, M.A.K., 2009. Determining the degree of methylesterification of pectin by ATR/FT-IR: methodology optimization and comparison with theoretical calculations. Carbohydr. Polym. 78, 847–853.

Freitas, F., Alves, V.D., Reis, M.A.M., 2011. Advances in bacterial exopolysaccharides: from production to biotechnological applications. Trends Biotechnol. 29 (8), 388–398.

González-Garcinuño, A., Masa, R., Hernandez, M., Dominguez, A., Tabernero, A., Martin del Valle, E., 2019. Levan-capped silver nanoparticles for bactericidal formulations: release and activity modelling. Int. J. Mol. Sci. 20, 1–19.

González-Garcinuño, A., Tabernero, A., Marcelo, G., Martin del Valle, E., 2020. A comprehensive study on levan nanoparticles formation: kinetics and self-assemby modeling. Int. J. Biol. Macromol. 147, 1089–1098.

Jathore, N.R., Bule, M.V., Tilay, A.V., Annapure, U.S., 2012. Microbial levan from *Pseudomonas fluorescens*: characterization and medium optimization for enhanced production. Food Sci. Biotcehnol. 21 (4), 1045–1053.

Kang, S.A., Jang, K., Seo, J., Kim, K.H., Kim, Y.H., Rairakhwada, D., Seo, M.Y., Lee, J.O., Ha, S.D., Kim, C., Rhee, S., 2009. Levan Applications and Perspective. Casister Academic Press, United Kingdom, pp. 145–157.

Kim, S.J., Chung, B.H., 2016. Antioxidant activity of levan coated cerium oxide nanoparticles. Cabohydr. Polym. 150, 400–4007.

Liu, J., Luo, J., Ye, H., Zeng, X., 2012. Preparation, antioxidant and antitumor activities *in vitro* of different derivatives of levan from endophytic bactrium *Paenibacillus polymyxa* EJS-3. Food Chem. Toxicol. 50, 767–772.

Mirza, A.Z., Siddiqui, F.A., 2014. Nanomedicine and drug delivery: a mini review. Int. Nano Lett. 4 (94), 1–7.

Murali, M., Mahendra, C., Nagabhushan, Rajashekar, N., Sudarshana, M.S., Raveesha, K.A., Amruthesh, K.N., 2017. Antibacterial and antioxidant properties of biosynthesized zinc oxide nanoparticles from *Ceropegia candalebrum* L. -An endemic species. Spectrochim. Acta Mol. Biomol. Spectrosc. 179, 104–109.

Nicolaus, B., Kambourova, M., Oner, E.T., 2010. Exopolysaccharides from extremophiles: from fundamentals to biotechnology. Environ. Technol. 31, 1145–1158.

Nwodo, E.G., Okoh, A., 2012. Bacterial exopolysaccharides: functionality and prospects. Int. J. Mol. Sci. 13 (12), 14002–14015.

Peng, C., Wang, X., Chen, J., Jiao, R., Wang, L., Li, Y.M., Zuo, Y., Liu, Y., Lei, L., Huang, Y., Chen, Z., 2014. Biology of aging and role of dietary antioxidants. BioMed Res. Int. 831841.

Pham-Huy, L.A., He, H., Pham-Huy, C., 2008. Free radicals, antioxidants in disease and health. Int. J. Biomed. Sci. 4 (2), 89–96.

Pudovkin, Maksim S., Zelenikhin, Pavel V., Shtyreva, Victoria, Morozov, Oleg A., Koryakovtseva, Darya A., Pavlov, Vitaly V., Osin, Yury N., Evtugyn, Vladimir G., Akhmadeev, Albert A., Nizamutdinov, Alexey S., Semashko, Vadim V., 2018. Coprecipitation Method of Synthesis, Characterization, and Cytotoxicity of Pr3+: LaF3 (CPr = 3, 7, 12, 20, 30%) Nanoparticles. J. Nanotechnol. 2018, 1–9.

Rehm, B.H.A., 2009. Microbial Production of Biopolymers and Polymer Precursors: Applications and Perspectives. Caister Academic Press, Caister, pp. 545–547.

Sarilmiser, H.K., Oner, E.T., 2014. Investigation of anti-cancer of linear and aldehyde-activated levan from *Halomonas smyrnensis* AAD6T. Biochem. Eng. J. 92, 28–34.

Srikanth, R., Siddartha, G., Reddy, C.H., Harish, B.S., Ramiah, M.J., Uppuluri, K.B., 2015. Antioxidant and anti-inflammatory levan produced from Acetobacter xylinum NCIM2526 and its statistical optimization. Carbohydr. Polym. 123, 8–16.

Sundaram, P.A., Augustine, R., Kannan, M., 2012. Extracellular biosynthesis of iron oxide nanoparticles by *Bacillus subtilis* strain isolated from rhizosphere soil. Biotechnol. Bioproc. Eng. 17, 835–840.

Valgimigli, L., Baschieri, Amorati, R., 2018. Antioxidant activity of nanomaterials. J. Mater. Chem. B 6, 2036–2051.

Zhao, G., Kan, J., Li, Z., Chen, Z., 2005. Structural features and immunological activity of a polysaccharide from Dioscorea opposita Thunb roots. Carbohydr. Polym. 61, 125–131.

Zhao, W., Zhang, J., Jiang, Y.Y., Zhao, X., Hao, X.N., Li, L., Yang, Z.N., 2018. Characterization and antioxidant activity of the exopolysaccharide produced by Bacillus amyloliquefaciens GSBa-1. *J.* Microbiol. Biotechnol. 28 (8), 1282–1292.